Local inversion of the sonar transform regularized by the approximate inverse

2011 Inverse Problems 27 035006

(http://iopscience.iop.org/0266-5611/27/3/035006)

IOP PUBLISHING INVERSE PROBLEMS

Inverse Problems **27** (2011) 035006 (18pp) doi:10.1088/0266-5611/27/3/035006

Local inversion of the sonar transform regularized by the approximate inverse

Eric Todd Quinto[1], **Andreas Rieder**[2] **and Thomas Schuster**[3]

[1] Department of Mathematics, Tufts University, Medford, MA 02155, USA
[2] Fakultät für Mathematik, Karlsruher Institut für Technologie (KIT), D-76128 Karlsruhe, Germany
[3] Fakultät V, Institut für Mathematik, Carl von Ossietzky Universität Oldenburg, 26111 Oldenburg, Germany

E-mail: todd.quinto@tufts.edu, andreas.rieder@kit.edu and thomas.schuster@uni-oldenburg.de

Received 26 September 2010, in final form 3 January 2011
Published 10 February 2011
Online at stacks.iop.org/IP/27/035006

Abstract

A new reconstruction method is given for the spherical mean transform with centers on a plane in $\mathbb{R}^3$ which is also called the sonar transform. Standard inversion formulas require data over all spheres, but typically, the data are limited in the sense that the centers and radii are in a compact set. Our reconstruction operator is local because, to reconstruct at $\mathbf{x}$, one needs only spheres that pass near $\mathbf{x}$, and the operator reconstructs singularities, such as object boundaries. The microlocal properties of the reconstruction operator, including its symbol as a pseudodifferential operator, are given. The method is implemented using the approximate inverse, and reconstructions are given. They are evaluated in light of the microlocal properties of the reconstruction operator.

(Some figures in this article are in colour only in the electronic version)

1. Introduction

In this paper, we develop a novel local reconstruction method for the spherical Radon transform with centers on a plane. As this transform is one model for sonar under the Born approximation, that is, under the assumption there are not multiple scattering events, it is also called the sonar transform.

Let $u(t, \mathbf{x})$ be the acoustic pressure field at $\mathbf{x} \in \mathbb{R}^3$ at time $t \geqslant 0$. Then, u satisfies the acoustic wave equation

$$\Delta_{\mathbf{x}} u - \frac{1}{v^2} \partial_t^2 u = -\delta(\mathbf{x} - \mathbf{z})\delta(t) \tag{1.1}$$

where $v = v(\mathbf{x})$ is the speed of sound and $\mathbf{z} \in \mathcal{P} = \{\mathbf{x} \in \mathbb{R}^3 \,|\, x_3 = 0\}$ is the excitation point on the ocean surface. The inverse problem in sonar is to recover v from the backscattered (reflected) field u_s observed at $\mathcal{P}$ for all times $t > 0$.

Cohen and Bleistein [3] made the ansatz

$$\frac{1}{v^2(\mathbf{x})} = \frac{1 + n(\mathbf{x})}{c^2}$$

where c is a constant background velocity. Then,

$$\frac{1}{4\pi}\frac{1}{c^2\tau^2}\int_{\mathcal{S}(\mathbf{y},\frac{c\tau}{2})} n(\mathbf{x})\,\mathrm{d}S(\mathbf{x}) = -c^2\int_0^\tau (\tau - t)u_s(t,\mathbf{y})\,\mathrm{d}t + \text{higher order terms in } n \tag{1.2}$$

where $\mathcal{S}(\mathbf{y}, r)$ is the sphere centered at $\mathbf{y} \in \mathbb{R}^3$ and of radius r and τ is the observation period. Under the assumption that $n \ll 1$ (i.e. the Born approximation), the higher order terms are set to zero and the right-hand side of (1.2) becomes an integral from 0 to τ of the solution to the wave equation. Thus, (1.2) reduces to recovering $n(\mathbf{x})$ from the integrals of n over spheres centered on the plane $\mathcal{P}$ where the right-hand side in (1.2) is known from the measured data $u(t, \mathbf{y})$.

Since we are interested in spheres with centers on the plane $x_3 = 0$, we define our spheres in terms of $\mathbf{z} \in \mathbb{R}^2$ and $r > 0$:

$$S(\mathbf{z}, r) = \{\mathbf{x} \in \mathbb{R}^3 \,|\, |\mathbf{x} - (\mathbf{z}, 0)| = r\}, \qquad Y = \{(\mathbf{z}, r) \,|\, \mathbf{z} \in \mathbb{R}^2, r > 0\}. \tag{1.3}$$

We define the *spherical Radon transform* for $(\mathbf{z}, r) \in Y$ to be the spherical mean over $S(\mathbf{z}, r)$:

$$Rn(\mathbf{z}, r) = \frac{1}{4\pi r^2}\int_{S(\mathbf{z},r)} n(\mathbf{x})\,\mathrm{d}S(\mathbf{x}). \tag{1.4}$$

Our goal is to use this spherical mean data to reconstruct a picture of n showing region boundaries. Since the null space of R is the set of odd functions [4], R is not injective for arbitrary functions on $\mathbb{R}^3$. This null space characterization implies that R is injective for functions supported in $x_3 > 0$. We let

$$\mathbb{R}^3_+ = \{\mathbf{x} \in \mathbb{R}^3 \,|\, x_3 > 0\}$$

and we will consider only functions supported in $\mathbb{R}^3_+$. This is a realistic assumption for functions in the ocean when we assume that $x_3 > 0$ points down to the ocean floor.

We define the backprojection operator R^* for compactly supported functions $g(\mathbf{z}, r)$ as

$$R^*g(\mathbf{x}) = \int_{\mathbb{R}^2} g(\mathbf{z}, |\mathbf{x} - (\mathbf{z}, 0)|)\,\mathrm{d}\mathbf{z}. \tag{1.5}$$

Note that

$$|\mathbf{x} - (\mathbf{z}, 0)| = \sqrt{|\mathbf{x}' - \mathbf{z}|^2 + x_3^2} \quad \text{where} \quad \mathbf{x}' = (x_1, x_2, x_3)' := (x_1, x_2).$$

The operator R^* is used in [2, 6] and it is the dual operator to R if the measure on $\mathbb{R}^3_+$ is $\mathrm{d}x$ and the measure on Y is $4\pi r^2\,\mathrm{d}r\,\mathrm{d}\mathbf{z}$. The problem is that one cannot define R^* on the range of R even for compactly supported functions f because Rf is not necessarily compactly supported even if f is. Therefore, we will need to include a cutoff function, see (2.2) below, in the definition of our reconstruction operator.

Inversion algorithms for this problem exist if data are known over all spheres with the center on a plane [2, 6, 13, 17]. For the two-dimensional problem, Palamodov [18] analyzed the visible and invisible singularities, providing seminorm strength estimates for each, and Denisjuk [5] developed inversion algorithms. Schuster and Quinto [25] adapted the approximate inverse to distributions and used it to develop an inversion algorithm for the two-dimensional problem. This model, integration over spheres, also comes up in thermoacoustic

and photoacoustic tomography, but in this case the centers are constrained to lie on a sphere or other surface that encloses the region to be imaged ([1, 11, 14, 27] provide references and background).

Our reconstruction operator is local in the sense that to reconstruct at a point $\mathbf{x}$, one needs only spheres that are near $\mathbf{x}$, and the operator is easily restricted to the data that are given in practice. Typical data are limited since one can acquire data only over a compact set in Y, and the authors know of no reconstruction method from this limited data in $\mathbb{R}^3$. Our reconstruction operator will detect singularities such as boundaries of the object rather than finding reflectivity values, and as shown in section 5, the operator can image objects clearly. Furthermore, our algorithm is easy to adapt to different data acquisition geometries, such as when $\mathbf{z}$ lies on an arbitrary C^∞ surface rather than a plane.

In section 2 we define our reconstruction operator and give its basic properties. To understand why and how our algorithm detects singularities we will analyze its (principal) symbol as a pseudodifferential operator (ΨDO) (section 3). In section 4 we use the approximate inverse to regularize our inversion operator. To this end we analytically compute a reconstruction kernel from a given mollifier (theorem 4.1). Finally, we present several fully 3D numerical experiments in section 5 and analyze the resulting reconstructions in the light of the microlocal results we developed in section 3. The technical proof of theorem 4.1 is given in the appendix.

2. Our local reconstruction operator

In contrast to the *planar* Radon transform that integrates over planes, the spherical Radon transform R cannot be formulated as a bounded operator between either appropriate L^2- or Sobolev spaces. Moreover Andersson [2] proves that R acts as a bounded mapping between suitable chosen spaces of tempered distributions. Let

$$\mathcal{S}_{\mathrm{e}}(\mathbb{R}^3) := \{f \in \mathcal{S}(\mathbb{R}^3) \,|\, f(\mathbf{x}', -x_3) = f(\mathbf{x}', x_3)\}$$

be the space of rapidly decreasing functions that are even in x_3 and let

$$\mathcal{S}_{\mathrm{r}}(\mathbb{R}^2 \times \mathbb{R}^3) = \{f \in \mathcal{S}(\mathbb{R}^5) \,|\, f(\mathbf{z}, w) = \check{f}(z, \|w\|) \text{ for a function } \check{f} \in \mathcal{S}_{\mathrm{e}}(\mathbb{R}^3)\}$$

be the space of rapidly decreasing functions in $\mathbb{R}^5$ that are radially symmetric in the last three components. The dual spaces $\mathcal{S}_{\mathrm{e}}(\mathbb{R}^3)'$ and $\mathcal{S}_{\mathrm{r}}(\mathbb{R}^2 \times \mathbb{R}^3)'$ of $\mathcal{S}_{\mathrm{e}}(\mathbb{R}^3)$ and $\mathcal{S}_{\mathrm{r}}(\mathbb{R}^2 \times \mathbb{R}^3)$, respectively, consist of tempered distributions. In general $f \in \mathcal{S}_{\mathrm{e}}(\mathbb{R}^3)$ does not imply that $Rf \in \mathcal{S}_{\mathrm{r}}(\mathbb{R}^2 \times \mathbb{R}^3)$, but it is easy to show that $Rf \in \mathcal{S}_{\mathrm{r}}(\mathbb{R}^2 \times \mathbb{R}^3)'$. By a density argument we derive that R maps $\mathcal{S}_{\mathrm{e}}(\mathbb{R}^3)'$ to $\mathcal{S}_{\mathrm{r}}(\mathbb{R}^2 \times \mathbb{R}^3)'$ and Andersson [2, theorem 2.1] proved that this gives a bounded operator whose dual operator maps $\mathcal{S}_{\mathrm{r}}(\mathbb{R}^2 \times \mathbb{R}^3)$ to $\mathcal{S}_{\mathrm{e}}(\mathbb{R}^3)$:

$$R^* : \mathcal{S}_{\mathrm{r}}(\mathbb{R}^2 \times \mathbb{R}^3) \to \mathcal{S}_{\mathrm{e}}(\mathbb{R}^3),$$

and has a dense range. As a consequence we see that the composition R^*R is not meaningfully defined in general and this is the reason for introducing a cutoff function ϕ in (2.2) below to obtain $\phi Rf \in \mathcal{S}_{\mathrm{r}}(\mathbb{R}^2 \times \mathbb{R}^3)$.

We use the following notation. Let Δ be the Laplacian in $\mathbb{R}^3$. We let H_{x_3} be the Hilbert transform in x_3 (the Fourier multiplier with symbol $-i\,\mathrm{sgn}(\xi_3)$ [26]), and we let $\partial_{x_3} = \partial/\partial x_3$.

Our local algorithm starts from an exact formula of Klein [13] that is based on the work of Andersson [2] and Fawcett [6]. The formula of Klein involves a modified dual operator that includes derivatives with respect to $\mathbf{x}$ of the data. He proves that the addition of the derivative allows one to compose the dual operator with R for functions in the range of R [13]. Klein's formula in $\mathbb{R}^3$ is

$$f = \frac{1}{2\pi} H_{x_3}(-\Delta)^{1/2} \int_{\mathbb{R}^2} (\partial_{x_3} Rf(\mathbf{z}, r)|_{r=|\mathbf{x}-(\mathbf{z},0)|})\, \mathrm{d}\mathbf{z}. \tag{2.1}$$

The integral in (2.1) is the R^* integral but with a ∂_{x_3} inside the integral. Fawcett [6] and Andersson [2, p 223] have a formula similar to (2.1), but they use the notation Δ for the *negative* Laplacian (see e.g. [2], in particular the formula for the Fourier transform at the bottom of p 222 and the inversion formula using Δ at the top of p 223).

Now we make (2.1) local. We replace $\frac{1}{2\pi}H_{x_3}$ (a pseudodifferential operator of order 0) by the identity, and we replace the nonlocal operator $(-\Delta)^{1/2}$ by $(-\Delta)$. The replacement of $(-\Delta)^{1/2}$ by $(-\Delta)$ increases the order of the operator from order 0 (the order of the identity) to order 1. Finally, we specify constants $0 < T' < T$ and $0 < \delta < \delta' < M' < M$ and choose a C^∞ cutoff in $\mathbf{z}$ and in r:

$$\begin{aligned} \phi : \mathbb{R}^2 \times (0,\infty) \to [0,1],\ \operatorname{supp}(\phi) = [-T,T]^2 \times [\delta, M], \\ \phi(\mathbf{z},r) > 0 \ \ (\mathbf{z},r) \in (-T,T)^2 \times (\delta, M), \\ \phi(\mathbf{z},r) = 1 \ \ (\mathbf{z},r) \in [-T',T']^2 \times [\delta', M']. \end{aligned} \tag{2.2}$$

Including ϕ allows us to compose R^* and R even when the data Rf are not compactly supported. Multiplying by $\phi(\mathbf{z},r)$ *before* using ∂_{x_3} allows us to bring the derivative ∂_{x_3} outside the R^* integral to get our reconstruction operator for $\mathbf{x} \in \mathbb{R}^3$:

$$\Lambda f(\mathbf{x}) := -\Delta \partial_{x_3} R^*(\phi(\mathbf{z},r) Rf(\mathbf{z},r))(\mathbf{x}). \tag{2.3}$$

This operator is a natural generalization of the Lambda tomography operator [7] since it is of order 1 as we will claim in theorem 3.2 and it is local in the following sense. To reconstruct $\Lambda f(\mathbf{x})$ one only needs spheres near $\mathbf{x}$ to calculate the derivatives and to evaluate R^*.

3. The microlocal properties of Λ and its symbol as a ΨDO

In this section, we give the microlocal properties of R. We prove Λ is a ΨDO on $\mathbb{R}^3_+$ and we give its symbol and where it is elliptic. This will show how much Λ emphasizes singularities in different directions. In order to understand what R and Λ do to singularities, we must first understand what singularities are and this will be framed in terms of the wavefront set.

For $f \in L^1(\mathbb{R}^n)$ we define the Fourier transform of f to be

$$\mathcal{F}f(\xi) = \frac{1}{(2\pi)^{n/2}} \int_{\mathbb{R}^n} f(\mathbf{x}) \exp(-\mathrm{i}\xi \cdot \mathbf{x})\, \mathrm{d}\mathbf{x}$$

and we note that $\mathcal{F}^{-1} f(\mathbf{x}) = \mathcal{F}f(-\mathbf{x})$. If $\mathcal{F}f$ is rapidly decreasing at ∞ (decreasing faster than any power of $1/|\xi|$ at ∞) then f and all its derivatives are continuous, that is, $f \in C^\infty(\mathbb{R}^n)$. This is the motivation for the definition of the wavefront set: we can understand the smoothness of f by understanding where a localized Fourier transform of f is rapidly decreasing at ∞. We note that a cutoff function at $\mathbf{x}_0$ will be any C^∞ compactly supported function $\varphi : \mathbb{R}^n \to [0,\infty)$ such that $\varphi(\mathbf{x}_0) \neq 0$.

Definition 3.1. *Let f be a distribution in $\mathbb{R}^n$ and let $\mathbf{x}_0 \in \mathbb{R}^n$ and $\xi_0 \in \mathbb{R}^n \setminus \mathbf{0}$. Then f is smooth at $\mathbf{x}_0$ in direction ξ_0 if for some cutoff function φ at $\mathbf{x}_0$ and some open conic neighborhood V of ξ_0, $\mathcal{F}(\varphi f)$ is rapidly decreasing at ∞ for $\xi \in V$.*

If f is not smooth at $\mathbf{x}_0$ in the direction ξ_0 then we say $(\mathbf{x}_0, \xi_0) \in \mathrm{WF}(f)$.

Definition 3.1 is given in [19, p 146] and it is equivalent to the one in the seminal article [12]. Using our next definition, we can evaluate qualitative strength of singularities using Sobolev weights.

Definition 3.2 ([19, p 258]). *Let f be a distribution in $\mathbb{R}^n$ and let $\mathbf{x}_0 \in \mathbb{R}^n$ and $\xi_0 \in \mathbb{R}^n \setminus \mathbf{0}$. Then f is in H^s at $\mathbf{x}_0$ in direction ξ_0 if for some cutoff function φ at $\mathbf{x}_0$ and some open conic neighborhood V of ξ_0, the microlocal Sobolev seminorm*

$$\|\varphi f\|_{H^s,V} = \sqrt{\int_V |\mathcal{F}(\varphi f)(\xi)|^2 (1+|\xi|^2)^s \, \mathrm{d}\xi}$$

is finite.

If f is not in H^s at $\mathbf{x}_0$ in direction ξ_0 then we say $(\mathbf{x}_0, \xi_0) \in \mathrm{WF}^s(f)$.

In general, the wavefront set and Sobolev wavefront sets are defined as subsets of the cotangent bundle $T^*(\mathbb{R}^n)$, because this allows one to define the wavefront set invariantly on manifolds. However, we will consider the wavefront of f as a subset of $\mathbb{R}^n \times \mathbb{R}^n \setminus \mathbf{0}$, since we will not consider manifolds besides $\mathbb{R}^n$ (except in the technical parts of the proof of theorem 3.2 and remark 3.3, where we will use cotangent bundles).

Note that if f is smooth on $\mathbb{R}^n$ then $\mathrm{WF}(f) = \emptyset$. If f is the characteristic function χ_Ω of a domain Ω with C^∞ boundary, then $\mathrm{WF}(\chi_\Omega)$ is the set of normal vectors to the boundary

$$N(\mathrm{bd}(\Omega)) = \{(\mathbf{x}, \xi) \,|\, \mathbf{x} \in \mathrm{bd}(\Omega),\ \xi \in \mathbb{R}^3 \setminus \mathbf{0},\ \xi \perp \mathrm{bd}(\Omega) \text{ at } \mathbf{x}\} = \mathrm{WF}(\chi_\Omega). \tag{3.1}$$

This is also true for $\mathrm{WF}^s(f)$ for $s \geqslant 1/2$.

Radon transforms detect singularities perpendicular to the set being integrated over and so R will detect singularities of f normal to the sphere being integrated over. This is made clear in the following theorem; a more precise version was given in [16] and was proven for manifolds in arbitrary dimensions in [21].

Theorem 3.1. *Let R be the spherical Radon transform in $\mathbb{R}^3$ with centers on the plane $x_3 = 0$. Then, R is an elliptic Fourier integral operator for functions supported in $\mathbb{R}^3_+$. Let f be a locally integrable function on $\mathbb{R}^3_+$ and $\mathbf{z} \in \mathbb{R}^2$ and $r > 0$. $\mathrm{WF}(f) \cap N(S(\mathbf{z}, r)) = \emptyset$ if and only if Rf is C^∞ in some neighborhood of $(\mathbf{z}, r)$.*

In [21] a precise relationship is given between the wavefront set of f and that of Rf, and the simple version given here explains that R 'sees' singularities only if they are normal to the sphere $S(\mathbf{z}, r)$.

Example 3.1. To illustrate our theorem, we give a basic example. Let f be the characteristic function of a domain $\Omega \subset \mathbb{R}^3_+$ with C^∞ boundary. According to theorem 3.1, a singularity of f will be visible in Rf near $(\mathbf{z}, r)$ if and only if the sphere $S(\mathbf{z}, r)$ is tangent to $\mathrm{bd}(\Omega)$ (so normals to the boundary are normal to the sphere). Our reconstructions in section 5 are from a limited set of spheres, and the only singularities that are visible in those reconstructions are the ones normal to spheres in the dataset. Palamodov referred to the wavefront directions normal to $S(\mathbf{z}, r)$ as *audible*, and he proved elegant estimates for singularities in the audible zone (and inaudible zone) for the circle transform in $\mathbb{R}^2$ [18].

Now that we have discussed the microlocal properties of R, we consider Λ. We first prove that Λ is a ΨDO and we give its symbol and then we discuss what the symbol means for the algorithm.

Theorem 3.2. *Let Λ be the operator (2.3) with the C^∞ cutoff function ϕ (2.2). Then, Λ is a pseudodifferential operator of order 1 on $\mathcal{E}'(\mathbb{R}^3_+)$. Furthermore the top-order symbol of Λ is*

$$\sigma(\Lambda) = 2\pi \mathrm{i} \phi\left(\left(\mathbf{x} - \frac{x_3}{\xi_3}\xi\right)', \frac{x_3}{|\xi_3|}|\xi|\right) \frac{\xi_3}{|\xi_3|}|\xi| \tag{3.2}$$

where $(y_1, y_2, y_3)' = (y_1, y_2)$.

Note that the argument of ϕ is not defined if $\xi_3 = 0$, but we define the symbol to be zero there since for each $x \in \mathbb{R}^3_+$, the symbol is zero for ξ_3 close to 0. Before we prove the theorem we make some observations about what this means for our problem.

Note that our domain is $\mathbb{R}^3_+$ and so x_3 is always positive. The operator Λ is not elliptic since $\sigma(\Lambda)$ can be zero as ϕ can be zero. For $\mathbf{x} \in \mathbb{R}^3_+$, let

$$C(\mathbf{x}) = \left\{ \xi \in \mathbb{R}^3 \,|\, \xi_3 \neq 0,\ \left(\mathbf{x} - \frac{x_3}{\xi_3}\xi\right)' \in (-T, T)^2,\ x_3|\xi|/|\xi_3| \in (\delta, M) \right\}. \tag{3.3}$$

The symbol of Λ is zero on the complement of $\mathrm{Cl}(C(\mathbf{x}))$. Where the symbol is zero tells where the operator Λ smooths, so Λf will not show any wavefront of f at $(\mathbf{x}, \xi)$ if $\xi \notin C(\mathbf{x})$ (see remark 3.3 below).

Since the symbol $\sigma(\Lambda)$ is nonzero on $C(\mathbf{x})$ and homogeneous of degree 1 in ξ, if $\xi \in C(\mathbf{x})$, then Λ is elliptic of order 1 at $(\mathbf{x}, \xi)$. Therefore, if $\xi \in C(\mathbf{x})$, then $(\mathbf{x}, \xi) \in \mathrm{WF}(\Lambda f)$ if and only if $(\mathbf{x}, \xi) \in \mathrm{WF}(f)$. Thus, the wavefront of f for $\xi \in C(\mathbf{x})$ will, in some sense, be visible in Λf. Since Λ has degree 1 and is elliptic on $C(\mathbf{x})$, singularities of Λf will be one degree less smooth in the Sobolev scale than those of f. Of course wavefront directions near $\mathrm{bd}(C(\mathbf{x}))$ might be reconstructed more weakly than those corresponding to where $\phi = 1$. This discussion proves the following corollary.

Corollary 3.1. *Let Λ be the operator (2.3) with the C^∞ cutoff function ϕ (2.2). Let $\mathbf{x} \in \mathbb{R}^3_+$ and let $\xi \in C(\mathbf{x})$. Then,*

$$(\mathbf{x}, \xi) \in \mathrm{WF}^s(f) \text{ if and only if } (\mathbf{x}, \xi) \in \mathrm{WF}^{s-1}(\Lambda f). \tag{3.4}$$

Finally, we should emphasize that theorem 3.2 and corollary 3.1 are valid because we are considering only functions supported on one side of the plane $x_3 = 0$. Since the null space of R is the set of odd functions about $x_3 = 0$, R cannot distinguish singularities above $(\mathbf{x}', x_3)$ from those above $(\mathbf{x}', -x_3)$. However, for functions supported in $\mathbb{R}^3_+$, this is not a problem.

Proof (Proof of theorem 3.2)**.** We will give an easy to understand explanation of the result and then we outline the proof.

For purposes of this heuristic discussion, we assume we can compose R^* and R and write $R^*\partial_{x_3} = \partial_{x_3} R^*$ without having the cutoff ϕ. These assumptions are wrong in general, but this calculation shows what result we should expect, and it will allow us to skip one step in the rigorous calculation. By Klein's formula, $Id = \frac{1}{2\pi} H_{x_3}(-\Delta)^{1/2}\partial_{x_3} R^* R$, and the symbol of Id is 1. Recall that $\sigma(H_{x_3}) = -\mathrm{isgn}(\xi_3) = -\mathrm{i}\xi_3/|\xi_3|$ and $H_{x_3}^{-1} = -H_{x_3}$ [26]. Our operator Λ without the cutoff ϕ is then $2\pi(-H_{x_3})(-\Delta)^{1/2}\mathrm{Id}$ and therefore the symbol of Λ without the ϕ is $2\pi\,\mathrm{i}\frac{\xi_3}{|\xi_3|}|\xi|$ which corresponds to (3.2) without the ϕ.

Because we will be using manifolds besides $\mathbb{R}^n$ in this proof, we will use the invariant conventions for wavefront sets and canonical relations and consider them as subsets of cotangent bundles. We will denote covectors as follows: for $\xi = (\xi_1, \xi_2, \xi_3)$ we denote $\xi\mathbf{dx} = \xi_1\mathbf{dx}_1 + \xi_2\mathbf{dx}_2 + \xi_3\mathbf{dx}_3$ and for $\eta = (\eta_1, \eta_2)$, $\eta\mathbf{dz} = \eta_1\mathbf{dz}_1 + \eta_2\mathbf{dz}_2$.

To prove the theorem rigorously, we add the cutoff ϕ and we calculate the symbol of the composition of the Fourier integral operators that make up Λ. This starts with the canonical relation of R. Then the canonical relation of R is [21][4]

$$\mathcal{C} = \left\{ \left(\mathbf{z}, r, \mathbf{x}; \alpha((\mathbf{x}' - \mathbf{z})\mathbf{dz} + r\mathbf{dr} - (\mathbf{x} - (\mathbf{z}, 0))\mathbf{dx})\right) | \mathbf{x} \in \mathbb{R}^3_+, (\mathbf{z}, r) \in Y, \alpha \neq 0 \right\}. \tag{3.5}$$

Since $\mathbf{x} \in \mathbb{R}^3_+$ we can specify global coordinates on $\mathcal{C}$ where we let $S^2_+ = \{\omega \in S^2 \,|\, \omega_3 > 0\}$

$$S^2_+ \times \mathbb{R}^2 \times (0, \infty) \times (\mathbb{R} \setminus 0) \ni (\omega, \mathbf{z}, r, \alpha) \mapsto (\mathbf{z}, r, \mathbf{z} + r\omega; \alpha(\omega'\mathbf{dz} + \mathbf{dr} - \omega\,\mathbf{dx})) \tag{3.6}$$

[4] Note that in formula (4.7) of [21], $r\mathbf{dr}$ should be $2r\mathbf{dr}$.

after factoring. Using these coordinates it is easy to show that the projection $\Pi_L : \mathcal{C} \to T^*Y \setminus \mathbf{0}$ is an injective immersion. This is the Bolker assumption (e.g. [20, equation (3.1)]) and it implies that $R^*\phi R$ is a pseudodifferential operator [9, 10]. Note that if we considered $\mathbf{x} \in \mathbb{R}^3$ we would need to enlarge $\mathcal{C}$ so that in coordinates (3.6), we would need to include $\omega \in S_0^2 = \{\tau \in S^2 \,|\, \tau_3 = 0\}$ and Π_L is not an immersion above such points.

Using (3.5) one sees that the projection to $T^*\mathbb{R}^3_+ \setminus \mathbf{0}$, $\Pi_R : \mathcal{C} \to T^*\mathbb{R}^3_+ \setminus \mathbf{0}$ is also injective and for $(\mathbf{x}, \xi\mathbf{dx}) \in T^*\mathbb{R}^3_+ \setminus \mathbf{0}$, $\xi_3 \neq 0$, we have

$$\Pi_R^{-1}(\mathbf{x}, \xi\ \mathbf{dx}) = (\mathbf{z}(\mathbf{x}, \xi), r(\mathbf{x}, \xi), \mathbf{x}; \alpha(\xi)(\omega'(\xi)\mathbf{dz} + \mathbf{dr} - \omega(\xi)\ \mathbf{dx})), \tag{3.7}$$

$$\mathbf{z}(\mathbf{x}, \xi) = \left(\mathbf{x} - \frac{x_3}{\xi_3}\xi\right)', \tag{3.8}$$

$$r(\mathbf{x}, \xi) = \frac{x_3}{|\xi_3|}|\xi|, \tag{3.9}$$

$$\alpha(\xi) = -\frac{\xi_3|\xi|}{|\xi_3|}, \qquad \omega(\xi) = \frac{\xi_3}{|\xi_3||\xi|}\xi \in S^2_+. \tag{3.10}$$

Since ξ must be normal to the sphere $S(\mathbf{z}, r)$, ξ must be parallel $\mathbf{x} - (\mathbf{z}, 0)$. This explains (3.8). A calculation using (3.8) and the fact $x_3 > 0$ justifies (3.9). Finally, because $\xi_3 \neq 0$ and $\omega_3(\xi)$ must be positive (if we require $\omega \in S^2_+$), (3.8) and (3.9) are used to prove (3.10).

To calculate the symbol of Λ one follows the outline in [20]. We let $Z = \{(\mathbf{z}, r, \mathbf{x}) \,|\, |(\mathbf{z}, 0) \ - \mathbf{x})| = r\}$ be the *incidence relation* of all spheres and points such that the point $\mathbf{x}$ is on the sphere $S(\mathbf{z}, r)$. We have already chosen the measure $\mathrm{d}m = \mathrm{d}\mathbf{x}$ on $\mathbb{R}^3_+$ and $\mathrm{d}n = 4\pi r^2\, \mathrm{d}r\ \mathrm{d}\mathbf{z}$ on Y. We choose the measure on Z to be $\mathrm{d}\mu = \sqrt{\phi(\mathbf{z}, r)}r^2\ \mathrm{d}r\ \mathrm{d}\mathbf{z}\ \mathrm{d}\omega$. As done by Guillemin [8] one uses these measures to define measures for the Radon transform and its dual. This gives the measure on $S(\mathbf{z}, r)$ as $\frac{\mathrm{d}\mu}{\mathrm{d}n} = \frac{\sqrt{\phi(\mathbf{z},r)}}{4\pi}\,\mathrm{d}\omega$ and the measure for the backprojection is $\frac{\mathrm{d}\mu}{\mathrm{d}\mathbf{x}} = \sqrt{\phi(\mathbf{z}, r)}\,\mathbf{dz}$ and so the Radon transform defined by this theory is $R' = \sqrt{\phi}R$ and the dual transform is $(R')^* = R^*\sqrt{\phi}$. Therefore, $(R')^*R' = R^*\phi R$, and this justifies our choices of $\mathrm{d}x$, $\mathrm{d}n$ and $\mathrm{d}\mu$.

The next part of the calculation is to write I_Z, integration over Z, as a Fourier integral distribution. To do this one chooses coordinates so that Z is locally defined by $w = 0$ where coordinates on Z are $(\tilde{z}, w)$. One then follows the mathematics on p 337 [20] to calculate the symbol of I_Z as a Fourier integral distribution as in the calculation of (15) in that article. One calculates that it is

$$\sigma(I_Z) = \frac{(2\pi)^2\phi(\mathbf{z}, r)\,\mathrm{d}x\,\mathrm{d}z\,\mathrm{d}\eta}{(4\pi)r^2\Pi_R^*(|\sigma_{\mathbb{R}^3}|^{3/2})\Pi_L^*(|\sigma_Y|^{3/2})}(\Pi_R^{-1}(\mathbf{x}, \xi\ \mathbf{dx})) \tag{3.11}$$

where $\sigma_{\mathbb{R}^3}$ and σ_Y are the canonical symplectic forms on $T^*\mathbb{R}^3$ and T^*Y. To calculate the pullbacks in (3.11) one lets $\lambda = \Pi_R^{-1}(\mathbf{x}, \xi\ \mathbf{dx})$ as given in (3.8)–(3.10) and one chooses a basis of $T_\lambda\mathcal{C}$ using the coordinates (3.6). Then, using (3.11) and this calculation of the pullbacks, we get

$$\sigma(R^*\phi R)(\mathbf{x}, \xi) = \frac{2\pi\phi\left((\mathbf{x} - \frac{x_3}{\xi_3}\xi)', \frac{x_3|\xi|}{|\xi_3|}\right)}{|\xi_3||\xi|} \tag{3.12}$$

and composing with $\partial_{x_3}(-\Delta)$, which has symbol $\mathrm{i}\xi_3|\xi|^2$, gives us the final result (3.2). Finally, one should note that there is a Maslov symbol ([12] which is discussed in the first full paragraph in [20, p 338]) but it must be constant because the naively calculated symbol at the start of the proof can be defined as a function (see also the discussion on [20, p 338]). Note that

different conventions for the definition of symbol can result in different constants in (3.2), but our conventions are chosen so as to agree with the naive calculations at the start of this proof. □

Remark 3.3. We will now use the symbol calculation in the proof of theorem 3.2 to explain why Λ is smoothing off of the set $C(\mathbf{x})$ (3.3). It is clear from the definition of $C(\mathbf{x})$ that the symbol $\sigma(\Lambda)$ is zero off of $C(\mathbf{x})$, but since $\sigma(\Lambda)$ is the top order symbol, this implies only that Λ smooths one degree more off of $C(\mathbf{x})$ than on $C(\mathbf{x})$ not that it is C^∞ smoothing.

We will use the following notation [12]: $\mathcal{C}^t$ is $\mathcal{C}$ but with the $T^*\mathbb{R}^3$ and T^*Y coordinates reversed, and for $A \subset T^*\mathbb{R}^3$,

$$\mathcal{C} \circ A = \{(\mathbf{z}, r, \eta) \in T^*Y \,|\, \exists (\mathbf{x}, \tau) \in A, \text{with} (\mathbf{z}, r, \mathbf{x}; \eta, \tau) \in \mathcal{C}\}.$$

We now show that Λ is smoothing off of $C(\mathbf{x})$. Let $\mathbf{x} \in \mathbb{R}^3_+$ and $\xi \notin C(\mathbf{x})$. First assume $\xi_3 \neq 0$. In this case one can see using (3.7)–(3.10) that $\Pi_L(\Pi_R^{-1}(\mathbf{x}, \xi \mathbf{dx})) = (\mathbf{z}, r, \eta)$ for some $(\mathbf{z}, r) \in Y$ and some $\eta \in T^*_{(\mathbf{z},r)}Y$. However, since $\xi \notin C(\mathbf{x})$ by (3.8)–(3.10), ϕ is zero in a neighborhood of $(\mathbf{z}, r)$. Therefore, ϕRf is C^∞ in a neighborhood of $(\mathbf{z}, r)$ and so $(\mathbf{z}, r, \eta) \notin \mathrm{WF}(\phi Rf)$. This shows that

$$(\mathbf{x}, \xi \mathbf{dx}) = \Pi_R\left(\Pi_L^{-1}\left(\Pi_L\left(\Pi_R^{-1}(\mathbf{x}, \xi \mathbf{dx})\right)\right)\right) = \Pi_R\left(\Pi_L^{-1}(\mathbf{z}, r, \eta)\right)$$

is not in $\mathrm{WF}(R^*(\phi Rf))$. Here we are using the following: Π_L and Π_R are injective; for $A \subset T^*\mathbb{R}^3_+ \setminus \mathbf{0}$, $\mathcal{C} \circ A = \Pi_L\left(\Pi_R^{-1}(A)\right)$ and for $B \subset T^*Y$, $\mathcal{C}^t \circ B = \Pi_R\left(\Pi_L^{-1}(B)\right)$; and finally the composition calculus for Fourier integral operators [12]: $\mathrm{WF}(\Lambda(f)) \subset \mathcal{C}^t \circ (\mathcal{C} \circ \mathrm{WF}(f))$. Therefore, Λ is smoothing in the codirection $(\mathbf{x}, \xi\, \mathbf{dx})$.

If $\xi_3 = 0$ then by inspecting the expression for $\mathcal{C}$, (3.5), $\Pi_R^{-1}(\mathbf{x}, \xi \mathbf{dx}) = \emptyset$ since $x_3 \neq 0$. Therefore, for this ξ, $\mathcal{C}^t \circ (\mathcal{C} \circ \{(\mathbf{x}, \xi \mathbf{dx})\}) = \emptyset$ and Λ is smoothing in the codirection $(\mathbf{x}, \xi\, \mathbf{dx})$.

4. The approximate inverse: Mollifier $e_{\mathbf{p},s,k}$ and reconstruction kernel $\psi_{\mathbf{p},s,k}$

For an implementation of our local reconstruction operator Λ we need to stabilize its numerical evaluation. Several approaches are possible. We follow ideas of the approximate inverse [15] as it provides a general and well-developed framework for the stable solution of operator equations of the first kind, see e.g. [22–24].

Instead of computing $\Lambda f(\mathbf{p})$ for $\mathbf{p} \in \mathbb{R}^3_+$ directly, we recover the smoothed version

$$\langle \Lambda f, e_{\mathbf{p},s,k} \rangle_{L^2(\mathbb{R}^3)} \tag{4.1}$$

where

$$e_{\mathbf{p},s,k}(\mathbf{x}) = C_{k,s} \begin{cases} (s^2 - d^2)^k : d < s, \\ 0 \qquad\quad : d \geqslant s, \end{cases} \qquad d = |\mathbf{x} - \mathbf{p}|,$$

serves as the mollifier with $s, k > 0$ and

$$C_{k,s} = \left(\int_{B_s(\mathbf{p})} (s^2 - d^2)^k \, \mathrm{d}V\right)^{-1} = \frac{\Gamma(k + 5/2)}{\pi^{3/2}\Gamma(k+1)s^{3+2k}}.$$

Observe that

$$\int_{\mathbb{R}^3} e_{\mathbf{p},s,k}(\mathbf{x}) \mathrm{d}\mathbf{x} = 1 \quad \text{and} \quad \operatorname{supp} e_{\mathbf{p},s,k} = B_s(\mathbf{p}).$$

Further, the inner product (4.1) can be expressed as a convolution integral:

$$\Lambda f * e_{\mathbf{0},s,k}(\mathbf{p}) = \langle \Lambda f, e_{\mathbf{p},s,k} \rangle_{L^2(\mathbb{R}^3)}.$$

The parameter $s > 0$ scales the mollifier and plays the role of a regularization parameter: the larger the s the smoother the reconstruction. In what follows we implicitly assume $s < p_3$ yielding $\operatorname{supp} e_{\mathbf{p},s,k} \subset \mathbb{R}^3_+$ for $\mathbf{p} \in \mathbb{R}^3_+$. Note that k is merely a design parameter.

In the following theorem we give analytically a so-called reconstruction kernel allowing the computation of $\langle \Lambda f, e_{\mathbf{p},s,k}\rangle_{L^2(\mathbb{R}^3)}$ from the spherical means of f.

Theorem 4.1. *We have that*

$$\langle \Lambda f, e_{\mathbf{p},s,k}\rangle_{L^2(\mathbb{R}^3)} = \langle Rf, \psi_{\mathbf{p},s,k}\rangle_{L^2(\mathbb{R}^2\times[0,\infty[,r^2\mathrm{d}\mathbf{z}\mathrm{d}r)} \tag{4.2}$$

with the reconstruction kernel

$$\begin{aligned}\psi_{\mathbf{p},s,k}(\mathbf{z},r) = \phi(\mathbf{z},r)\frac{C_{k,s}kp_3A^{k-2}}{L}\Bigg[(2k+1)A\left[\frac{1}{Lk}\left(k-2+\frac{B}{2rL}\right)-\frac{1}{r}\right]\\ +2(k-1)s^2\left[\frac{1}{r}-\frac{1}{L(k-1)}\left(k-3+\frac{B}{2rL}\right)\right]\Bigg]\end{aligned} \tag{4.3}$$

for $r \in [L-s, L+s]$ *where*

$$L = |(\mathbf{z},0)-\mathbf{p}|, \quad A = s^2-(L-r)^2 \text{ and } B = (r+L)^2-s^2.$$

For $r \notin [L-s, L+s]$*:* $\psi_{\mathbf{p},s,k}(\mathbf{z},r) = 0$.

The proof of the theorem can be found in the appendix.

5. Reconstructions

In this section we give numerical reconstructions using the approximate inverse. We will also interpret the results in terms of the microlocal properties of R and Λ that were given in section 3.

We want to approximate

$$\Lambda f(\mathbf{p}) \approx \langle \Lambda f, e_{\mathbf{p},s,k}\rangle_{L^2(\mathbb{R}^3)} = \langle Rf, \psi_{\mathbf{p},s,k}\rangle_{L^2(\mathbb{R}^2\times[0,\infty[,r^2\,\mathrm{d}\mathbf{z}\mathrm{d}r)} \tag{5.1}$$

from the discrete data

$$g(i,j,k) = Rf(\mathbf{z}_{i,j}, r_k), \quad i,j = 1,\dots,N_{\mathrm{z}},\ k = 1,\dots,N_{\mathrm{r}}, \tag{5.2}$$

where

$$\{\mathbf{z}_{i,j}\} \subset [-z_{\max}, z_{\max}]^2 \quad \text{and} \quad \{r_k\} \subset (0, r_{\max}] \tag{5.3}$$

are Cartesian grids with uniform step sizes h_{z} and h_{r}, respectively. A straightforward discretization of the triple integral on the right of (5.1) yields

$$\begin{aligned}\Lambda f(\mathbf{p}) \approx \widetilde{\Lambda} f(\mathbf{p}) &:= h_{\mathrm{z}}^2 h_{\mathrm{r}} \sum_{i=1}^{N_{\mathrm{z}}}\sum_{j=1}^{N_{\mathrm{z}}}\sum_{k=1}^{N_{\mathrm{r}}} g(i,j,k)\psi_{\mathbf{p},s,k}(\mathbf{z}_{i,j}, r_k)r_k^2\\ &= h_{\mathrm{z}}^2 h_{\mathrm{r}} \sum_{i=1}^{N_{\mathrm{z}}}\sum_{j=1}^{N_{\mathrm{z}}}\sum_{r_k\in\mathcal{L}_{i,j}(\mathbf{p})} g(i,j,k)\psi_{\mathbf{p},s,k}(\mathbf{z}_{i,j}, r_k)r_k^2\end{aligned}$$

with $\mathcal{L}_{i,j}(\mathbf{p}) = [L-s, L+s]$ and $L = |(\mathbf{z}_{i,j},0)-\mathbf{p}|$. Thus, the numerical effort for computing $\widetilde{\Lambda} f(\mathbf{p})$ takes $\mathrm{O}(sN_{\mathrm{z}}^2)$ floating point operations when neglecting the evaluation of the kernel $\psi_{\mathbf{p},s,k}$ at $(\mathbf{z}_{i,j}, r_k)$. Note that the computation of $\widetilde{\Lambda} f$ at different reconstruction points can be done in parallel.

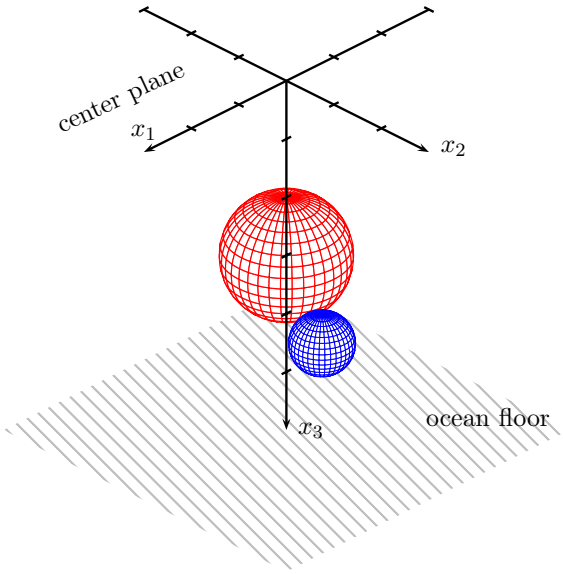

Figure 1. Visualization of the function (5.4) to be reconstructed. The two balls slightly intersect.

For our numerical computations presented in this section we have chosen the following cutoff function ϕ (2.2). Given $0 < \delta < \overline{M}$ and $\overline{T} > 0$ we define

$$\phi(\mathbf{z}, r) = \alpha(\mathbf{z})\beta(r)$$

where

$$\beta(r) = \begin{cases} 0 & : r \leqslant \delta \text{ or } r \geqslant \overline{M} + 1, \\ 1 & : \quad 2\delta \leqslant r \leqslant \overline{M}, \\ p(r, \overline{M}) & : \quad \overline{M} < r < \overline{M} + 1, \\ q(r, \delta) & : \quad \delta < r < 2\delta, \end{cases}$$

with

$$p(r, \overline{M}) = \frac{u(\overline{M} + 1 - r)}{u(\overline{M} + 1 - r) + u(r - \overline{M} - 1/2)}, \quad q(r, \delta) = \frac{u(r/\delta - 1)}{u(r/\delta - 1) + u(2 - r/\delta)},$$

and

$$u(x) = \begin{cases} \exp(-1/x) : x > 0, \\ 0 \qquad\quad : x \leqslant 0. \end{cases}$$

Further,

$$\alpha(\mathbf{z}) = \tilde{\alpha}(z_1)\tilde{\alpha}(z_2) \text{ and } \tilde{\alpha}(x) = \begin{cases} 1 & : \quad |x| < \overline{T}, \\ p(|x|, \overline{T}) & : \overline{T} \leqslant |x| \leqslant \overline{T} + 1, \\ 0 & : \quad |x| > \overline{T} + 1. \end{cases}$$

Thus,

$\phi \in C^\infty(\mathbb{R}^3)$, supp $\phi \subset [-\overline{T} - 1, \overline{T} + 1]^2 \times [\delta, \overline{M} + 1]$ and $\phi|_{[-\overline{T}, \overline{T}]^2 \times [2\delta, \overline{M}]} = 1$.

We always set $\overline{M} := r_{\max} - 1$, $\delta := 0.01$ and $\overline{T} := z_{\max} - 1$.

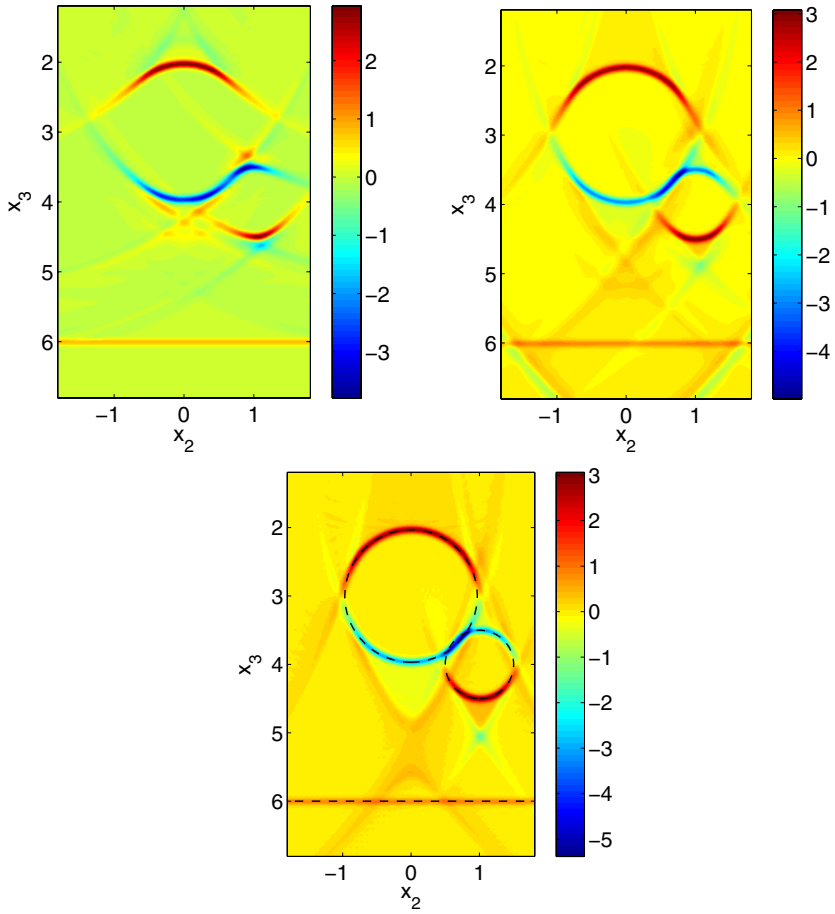

Figure 2. Reconstructions $\widetilde{\Lambda} f(0.25, \cdot, \cdot)$, f from (5.4), where $r_{\max} = 10$ and $z_{\max} = 3$ (top left), $z_{\max} = 6$ (top right) and $z_{\max} = 12$ (bottom) with $N_z = 301$ and $N_r = 250$, see (5.2) and (5.3). The parameters used for the reconstruction kernel are $s = 0.8$ and $k = 3$. The dashed black lines in the bottom reconstruction indicate the singular support of f and are not part of the reconstruction.

The function $f : \mathbb{R}^3_+ \to \mathbb{R}$ to be reconstructed is a superposition of three-indicator functions given by

$$f = \chi_{B_1(0,0,3)} - \chi_{B_{0.5}(0.25,1,4)} + 0.3\chi_{x_3 \geqslant 6} \tag{5.4}$$

whose sonar transform can be calculated analytically. The rightmost indicator function models a flat ocean floor at $x_3 = 6$, see figure 1 for a visualization.

In our first set of experiments we will demonstrate which singularities of f can be detected depending on the available data. To this end we note that the wavefront set of f (compare (3.1)) is

$$\begin{aligned}\mathrm{WF}(f) = {} & \{(\mathbf{x}, \xi) | \mathbf{x} \in \partial B_1(0, 0, 3),\ \xi = \lambda(\mathbf{x} - (0, 0, 3)),\ \lambda \neq 0\} \\ & \cup \{(\mathbf{x}, \xi) | \mathbf{x} \in \partial B_{0.25}(0.25, 1, 4),\ \xi = \lambda(\mathbf{x} - (0.25, 1, 4)),\ \lambda \neq 0\} \\ & \cup \{(\mathbf{x}, \xi) | x_3 = 6,\ \xi_1 = \xi_2 = 0,\ \xi_3 \neq 0\},\end{aligned}$$

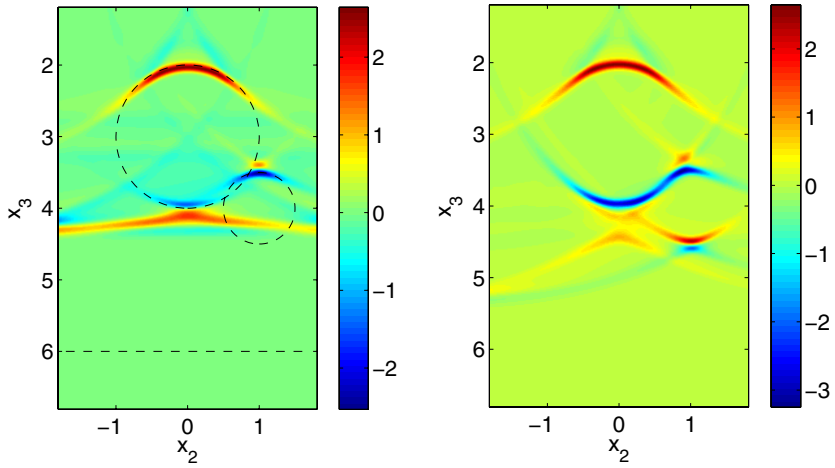

Figure 3. Cross sections $\widetilde{\Lambda} f(0.25, \cdot, \cdot)$, f from (5.4), where $r_{\max} = 4.5$ (left) and $r_{\max} = 5.5$ (right). Further, $z_{\max} = 3$, $N_z = 301$ and $N_r = 200$, see (5.2) and (5.3). The parameters used for the reconstruction kernel are $s = 0.8$ and $k = 3$. The dashed black lines in the left reconstruction indicate the singular support of f and are not part of the reconstruction.

that is, the wavefront set consists of all pairs $(\mathbf{x}, \xi)$ where $\mathbf{x}$ is on the boundary of either one of the two balls or of the ocean floor and ξ is normal to the boundary at this point[5].

Figure 2 displays cross sections $\widetilde{\Lambda} f(0.25, \cdot, \cdot)$ for three different sets of limited data: $z_{\max} = 3$ (top left), $z_{\max} = 6$ (top right) and $z_{\max} = 12$ (bottom). Further, $r_{\max} = 10$ in all three settings. All cross sections have been computed from $N_z^2 N_r = 301^2 \cdot 250 = 22,650,250$ spherical means.

To understand the extent to which our results from section 3 are reflected in our reconstructions, we inspect the set $C(\mathbf{x})$ (3.3) on which Λ is elliptic of order 1. The wavefront $(\mathbf{x}, \xi) \in \mathrm{WF}(f)$ will be visible in Λf (or $\widetilde{\Lambda} f$) if $\xi \in C(\mathbf{x})$, that is, $\xi_3 \neq 0$ and

$$\frac{x_i - z_{\max}}{x_3} < \frac{\xi_i}{\xi_3} < \frac{x_i + z_{\max}}{x_3}, \ i = 1, 2, \quad \text{and} \quad \frac{\delta}{x_3} < \frac{|\xi|}{|\xi_3|} < \frac{r_{\max}}{x_3}.$$

Thus, wavefronts for which ξ has dominant horizontal components ($|\xi_3|$ is small compared to $|\xi|$) will not be recovered. The visible wavefronts have dominant vertical components and the smaller $z_{\max}$ and $r_{\max}$ are and the larger x_3 is, the more dominant the vertical components have to be to be visible.

This fact is illustrated by the reconstructions shown in figures 2. With increasing $z_{\max}$ (top-left, top-right, bottom) more and more singularities of f are recovered. In the bottom reconstruction only the singularities with almost horizontal directions are missing. The ocean floor $\{(\mathbf{x}, \xi) | x_3 = 6, \ \xi_1 = \xi_2 = 0, \ \xi_3 \neq 0\}$ is visible because we have

$$\frac{x_i - z_{\max}}{6} < 0 < \frac{x_i + z_{\max}}{6} \ (\Leftrightarrow -z_{\max} < x_i < z_{\max}) \quad \text{and} \quad \frac{0.01}{6} < 1 < \frac{10}{6}.$$

In figure 3 we again display $\widetilde{\Lambda} f(0.25, \cdot, \cdot)$ with $z_{\max} = 3$, however, with clearly reduced maximal radii: $r_{\max} = 4.5$ and $r_{\max} = 5.5$. The ocean floor is not recovered by either reconstruction. For $r_{\max} = 4.5$ even the bottom hemisphere of the smaller ball is missing and a strong artifact corrupts the reconstruction.

[5] The two-boundary spheres intersect in a small circle. At each intersection point are two 'singularity directions' corresponding to normals to the two spheres.

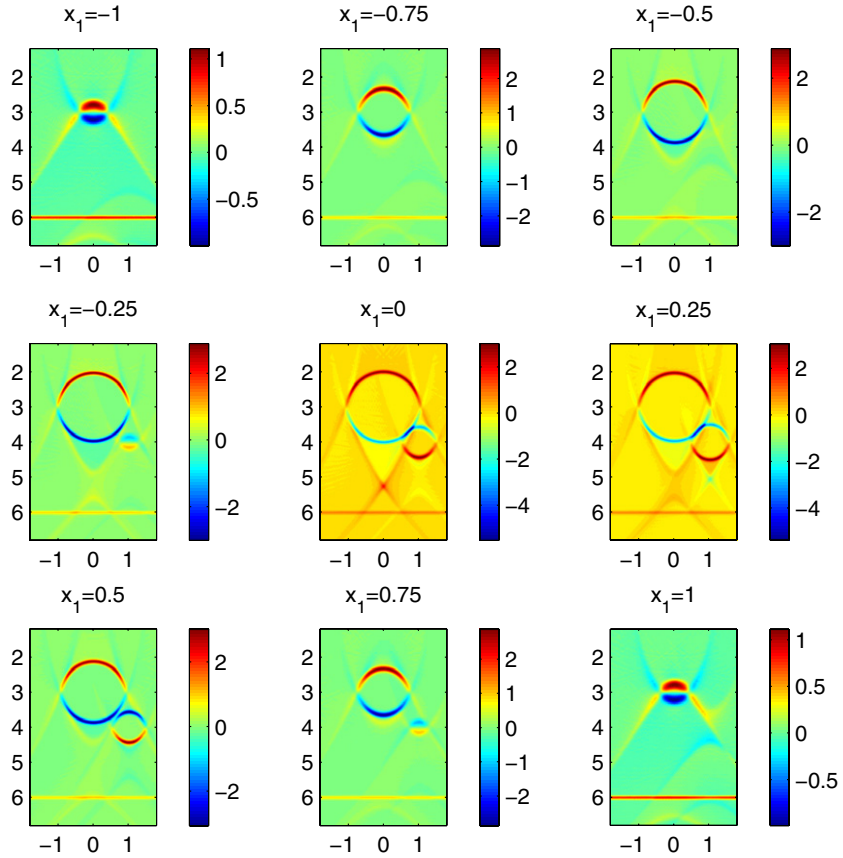

Figure 4. Cross sections $\widetilde{\Lambda} f(x_1, \cdot, \cdot)$, f from (5.4), for several x_1's. Here, $r_{\max} = 10$, $z_{\max} = 12$, $N_z = 301$ and $N_r = 250$, see (5.2) and (5.3). The parameters used for the reconstruction kernel are $s = 0.8$ and $k = 3$. Please note the different color scales for each reconstruction.

We have realized the evaluation of $\widetilde{\Lambda} f$ in a subroutine written in the C programming language and compiled by the `mex`-command under MATLAB 7.8 (R2009a). Within this MATLAB environment each of the reconstructions from figure 2 required about 12 h 30 min CPU-time on an AMD Athlon(tm) 64 Processor 3800+ with 2.5 GHz and 1 GB RAM where $\widetilde{\Lambda} f(0.25, \cdot, \cdot)$ has been computed on a 200×400 grid. Most of the CPU-time was consumed by evaluating the reconstruction kernel. Precomputing the kernel together with a clever interpolation scheme might reduce the run time considerably.

To prove that we really perform fully 3D reconstructions we display several cross sections $\widetilde{\Lambda} f(x_{1,i}, \cdot, \cdot)$ for $x_{1,i} = -1 + 0.25i$, $i = 0, \ldots, 8$, in figure 4. Here we like to emphasize the following observation: the boundaries of the two balls in the different cross sections are reconstructed with different intensities (note the different color (gray) scales). The reason for this fact is that the 3D-direction of the corresponding wavefront does not agree with the 2D-normal on the ball in the displayed cross section[6]. The more the wavefront direction

[6] We have two exceptions: for $x_1 = 0$ the 2D-normals on the large ball in the cross section agree with the corresponding directions of the wavefronts. The same holds true for the small ball at $x_1 = 0.25$.

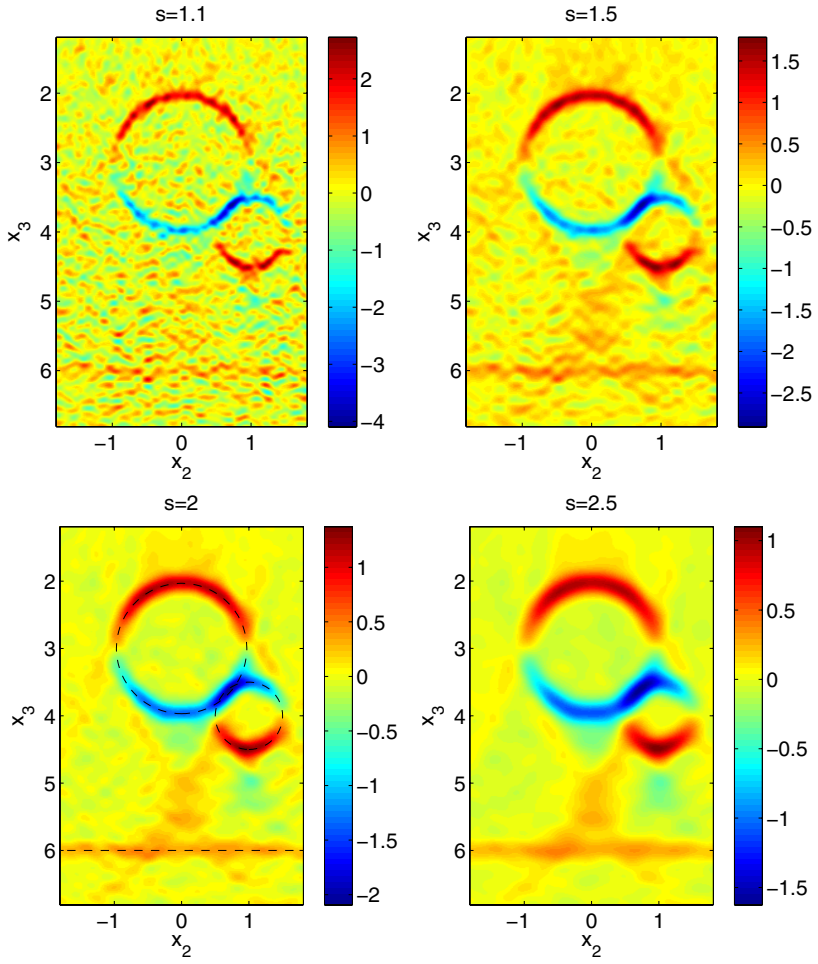

Figure 5. Reconstructions $\widetilde{\Lambda} f(0.25, \cdot, \cdot)$, f from (5.4), under 3% relative noise for different scaling parameters: $s = 1.1$ (top-left), $s = 1.5$ (top-right), $s = 2$ (bottom-left) and $s = 2.5$ (bottom-right). Further, $r_{\max} = 10$, $z_{\max} = 12$, $N_z = 301$, $N_r = 250$, see (5.2) and (5.3), and $k = 3$. The dashed black lines in the bottom-left reconstruction indicate the singular support of f and are not part of the reconstruction.

differs from the 2D-normal in the cross section the less pronounced is the singularity in the respective cross section.

We finish the numerics section by demonstrating how the algorithm performs with noisy data. To this end we perturb the exact data g (5.2) according to

$$g^{\varepsilon}(i, j, k) = g(i, j, k) + \varepsilon \|g\|_{\star} \frac{\texttt{noise}(i, j, k)}{\|\texttt{noise}\|_{\star}}, \quad \varepsilon > 0,$$

where `noise` is an $N_z \times N_z \times N_r$ array of uniformly distributed random numbers[7] with values in $[-1, 1]$ and where the discrete norm

$$\|g\|_{\star}^2 := h_z^2 h_r \sum_{i=1}^{N_z} \sum_{j=1}^{N_z} \sum_{k=1}^{N_r} |g(i, j, k)|^2 r_k^2$$

[7] In all computations we used the same `noise` array.

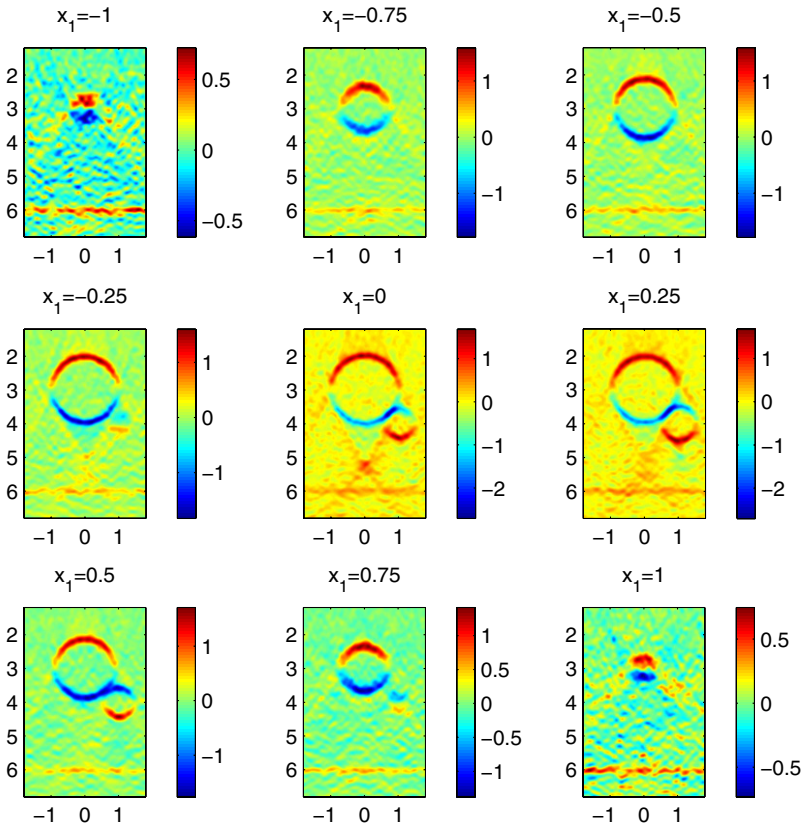

Figure 6. Cross sections $\widetilde{\Lambda} f(x_1, \cdot, \cdot)$, f from (5.4), for several x_1's under 3% relative noise. Here, $r_{\max} = 10$, $z_{\max} = 12$, $N_z = 301$ and $N_r = 250$, see (5.2) and (5.3). The parameters used of the reconstruction kernel are $s = 1.6$ and $k = 3$. Please note the different color scales for each reconstruction.

approximates the norm in $L^2\big([-\mathbf{z}_{\max}, \mathbf{z}_{\max}]^2 \times [0, r_{\max}], r^2\, \mathrm{d}\mathbf{z}\, \mathrm{d}r\big)$. We have that

$$\frac{\|g - g^\varepsilon\|_\star}{\|g\|_\star} \leqslant \varepsilon.$$

Thus, ε measures the *relative noise*. In all experiments below we worked with $\varepsilon = 3\%$.

First, the smoothing or regularizing effect of the scaling parameter s is illustrated. Figure 5 contains reconstructions of a cross section ($x_1 = 0.25$) from the same perturbed data for four different scaling parameters. As s increases the noise gets reduced at the price of blurred and fuzzy contours.

Finally, in figure 6 we present the same cross sections of $\widetilde{\Lambda} f$ as in figure 4, however, reconstructed from noisy data with the scaling parameter $s = 1.6$.

At the moment we lack a rigorous theory for selecting the regularization parameter s as a function of the discretization step sizes h_z and h_r and on the noise level ε. The asymptotic theory developed in [22] cannot straightforwardly extended to the present situation. Therefore, in our numerical experiments we have chosen s by trial and error inspecting the reconstructions visually. Such a selected parameter s for a certain configuration h_z, h_r, ε, noise characteristic and f is anticipated to deliver decent reconstructions also for different f that are of the same smoothness class. We propose this *modus operandi* in real applications.

Acknowledgments

The first author was supported in part by NSF Grant DMS 0908015 (and DMS 0456858 for preliminary work) and the Alexander von Humboldt Stiftung. The first author thanks Karlsruher Institut für Technologie (formerly Universität Karlsruhe) for its hospitality while this work was begun. The authors thank both referees for very helpful comments. They thank one of the referees for pointing out that (2.1) needed $(-\Delta)^{1/2}$ rather than $\Delta^{1/2}$. This error was due to a nonstandard convention for the Laplacian in [6] and [2].

Appendix. The proof of theorem 4.1

To find $\psi_{\mathbf{p},s,k}$, we start from (4.2) and by duality, we must have

$$\psi_{\mathbf{p},s,k}(\mathbf{z},r) = \phi(\mathbf{z},r)R(\partial_{x_3}\Delta e_{\mathbf{p},s,k})(\mathbf{z},r). \tag{A.1}$$

So as not to deal with too many constants, we consider an unnormalized version of $e_{\mathbf{p},s,k}$ and define

$$\tilde{e}_{\mathbf{p},s,k} = e_{\mathbf{p},s,k}/C_{k,s}.$$

Now we state the pieces we need to prove the expression for $\psi_{\mathbf{p},s,k}$ in theorem 4.1, and we use (A.1).

Lemma 5.1. *Let $k \in \mathbb{N}$, $k \geqslant 3$. Then,*

$$\begin{aligned} R(\partial_{x_3}\Delta\tilde{e}_{\mathbf{p},s,k})(\mathbf{z},r) &= [4k(2k+1)(k-1)[R(x_3\tilde{e}_{\mathbf{p},s,k-2}) - p_3R(\tilde{e}_{\mathbf{p},s,k-2})] \\ &\quad + 8k(k-1)(k-2)s^2[p_3R(\tilde{e}_{\mathbf{p},s,k-3}) - R(x_3\tilde{e}_{\mathbf{p},s,k-3})]]. \end{aligned} \tag{A.2}$$

For ℓ a nonnegative integer

$$R\tilde{e}_{\mathbf{p},s,\ell}(\mathbf{z},r) = \frac{A^{\ell+1}}{4(\ell+1)rL} \quad r \in (L-s, L+s) \tag{A.3}$$

and

$$R(x_3\tilde{e}_{\mathbf{p},s,\ell})(\mathbf{z},r) = \frac{p_3A^{\ell+1}}{4L^2(\ell+1)(\ell+2)}\left(\ell + \frac{B}{2rL}\right) \quad r \in (L-s, L+s). \tag{A.4}$$

where $L = |(\mathbf{z},0) - \mathbf{p}|$, $A = s^2 - (L-r)^2$ and $B = (r+L)^2 - s^2$ and where $r \in (L-s, L+s)$ and the functions in (A.3) and (A.4) are zero outside this interval.

The proof of (A.2) follows by a calculation and for $k = 3$ noting that the derivatives are distributional derivatives (since $\tilde{e}_{\mathbf{p},s,0}$ is not continuous). Using (A.3) and (A.4) for various values of ℓ in (A.2), one proves (4.3) in theorem 4.1.

To prove the lemma, first recall that $\mathbf{p}$ is the center of the mollifier $\tilde{e}_{\mathbf{p},s,\ell}$. We assume the sphere we are integrating over has radius r and is centered at $\mathbf{z} = (z_1, z_2)$ on the x_1x_2-plane. Furthermore, we denote the distance from $\mathbf{z}$ to $\mathbf{p}$ by

$$L := |(\mathbf{z},0) - \mathbf{p}|.$$

The condition for the integral to be nonzero is $r \in (L-s, L+s)$, so assume r is in this interval. Also, $L \geqslant p_3$ since $\mathbf{z}$ is on the x_1x_2-plane and $p_3 > 0$.

The calculation of $R(\partial_{x_3}\Delta\tilde{e}_{\mathbf{p},s,k})$ reduces to expressions involving $R(\tilde{e}_{\mathbf{p},s,\ell})$ and $R(x_3\tilde{e}_{\mathbf{p},s,\ell})$ for $\ell = k-3, k-2, k-1$ if one uses that $\tilde{e}_{\mathbf{p},s,k}$ is radial about $\mathbf{p}$, and one uses the radial form of the Laplacian $\Delta = \frac{\partial^2}{\partial d^2} + \frac{2}{d}\frac{\partial}{\partial d}$ where $d = |\mathbf{x} - \mathbf{p}|$. One uses this observation to calculate (A.2).

We now prove (A.4) by rotating and translating the picture and then using spherical coordinates. The proof of (A.3) uses similar arguments but is simpler. If we take a point $\mathbf{v}$ on $S(\mathbf{z}, r)$ then the x_3 coordinate of $\mathbf{v}$ is simply $\mathbf{v} \cdot e_3$. This is the same as

$$x_3 = \mathbf{v} \cdot e_3 = (\mathbf{v} - \mathbf{z}) \cdot e_3$$

since $\mathbf{z}$ is on the x_1x_2-plane.

Let $\alpha \in (0, \pi/2]$ be the angle between the vectors $((\mathbf{p}', 0) - \mathbf{z})$ and $(\mathbf{p} - \mathbf{z})$. Note that

$$\sin\alpha = p_3/L\,. \tag{A.5}$$

We make a rigid motion of $\mathbb{R}^3$ so that $(\mathbf{z}, 0)$ is mapped to the origin, $\mathbf{p}$ to $(0, 0, L)$ and $(\mathbf{p}', 0)$ to the point in the x_1x_3-plane:

$$(0, 0, L) + p_3(\cos\alpha, 0, -\sin\alpha).$$

Under this transformation, e_3 is mapped to the unit vector in the direction from $(0, 0, L) - x_3(\cos\alpha, 0, -\sin\alpha)$ to $(0, 0, L)$. That is,

$$e_3 \mapsto (-\cos\alpha, 0, \sin\alpha). \tag{A.6}$$

If $\mathbf{v} \in S(\mathbf{z}, r)$ let $\tilde{\mathbf{v}}$ be the point on $S(0, r)$ to which it is mapped under this rotation. Then the x_3-coordinate of $\mathbf{v}$ is

$$x_3 = \mathbf{v} \cdot e_3 = (\mathbf{v} - (\mathbf{z}, 0)) \cdot e_3 = (\tilde{\mathbf{v}} - (0, 0, 0)) \cdot (-\cos\alpha, 0, \sin\alpha) \tag{A.7}$$

since the dot product does not change under rigid motion and because under this rigid motion e_3 gets mapped to the vector in (A.6).

We can use spherical coordinates about the x_3-axis to integrate so an arbitrary point on the sphere of radius r centered at the origin is

$$(\theta, \phi) \mapsto \tilde{\mathbf{v}} = r(\cos\theta\sin\phi, \sin\theta\sin\phi, \cos\phi).$$

Using (A.7), we see that, in these new coordinates, x_3 is

$$\begin{aligned} x_3 &= r(\cos\theta\sin\phi, \sin\theta\sin\phi, \cos\phi) \cdot (-\cos\alpha, 0, \sin\alpha) \\ &= -r\cos\alpha\sin\phi\cos\theta + r\cos\phi\sin\alpha. \end{aligned}$$

When we put this into the integral of the spherical mean, we get

$$\begin{aligned} R(x_3\tilde{e}_{\mathbf{p},s,\ell})(\mathbf{z}, r) = \frac{1}{4\pi}\int_{\phi=0}^{\Phi}\int_{\theta=0}^{2\pi}[-r\cos\alpha\sin\phi\cos\theta + r\cos\phi\sin\alpha] \\ \times (s^2 - d^2)^\ell \sin\phi\,\mathrm{d}\theta\,\mathrm{d}\phi \end{aligned} \tag{A.8}$$

where Φ is the upper limit of integration. Since Φ is the angle at the origin of the triangle with vertices the origin and $(0, 0, L)$, and with sides r, L s, the law of cosines shows that

$$\begin{aligned} s^2 &= r^2 + L^2 - 2rL\cos\Phi, \\ \cos\Phi &= \frac{L^2 + r^2 - s^2}{2rL}. \end{aligned} \tag{A.9}$$

Now, we do some simple calculations. First, recall that in integral (A.8), ϕ is the angle of inclination from the x_3-axis to the point being integrated, so $d^2 = r^2 + L^2 - 2rL\cos\phi$ and using (A.9) we see

$$s^2 - d^2 = 2rL(\cos\phi - \cos\Phi) \tag{A.10}$$

and integral (A.8) becomes

$$\begin{aligned} R(x_3\tilde{e}_{\mathbf{p},s,\ell})(\mathbf{z}, r) = \frac{(2rL)^\ell}{4\pi}\int_{\phi=0}^{\Phi}\int_{\theta=0}^{2\pi}[-r\cos\alpha\sin\phi\cos\theta + r\cos\phi\sin\alpha] \\ \times (\cos\phi - \cos\Phi)^\ell \sin\phi\,\mathrm{d}\theta\,\mathrm{d}\phi. \end{aligned}$$

First, note that after we integrate in θ, the first term in brackets drops out, so we are left with

$$R(x_3\tilde{e}_{\mathbf{p},s,\ell})(\mathbf{z},r) = \frac{r(2rL)^\ell}{2}\int_{\phi=0}^{\Phi}[\cos\phi\sin\alpha](\cos\phi-\cos\Phi)^\ell\sin\phi\,\mathrm{d}\phi.$$

Now, if we make the substitution $u = \cos\phi - \cos\Phi$ (and $\cos\phi = u + \cos\Phi$) and use the expression (A.5) for $\sin\alpha$, then we get (A.4).

If one goes through a calculation using the same steps but without the factor of x_3, then one gets (A.3). In both (A.3) and (A.4), it helps to simplify $1-\cos\Phi$ and $1+\cos\Phi$ using (A.9).

References

[1] Agranovsky M, Kuchment P and Kunyansky L 2009 On reconstruction formulas and algorithms for the thermoacoustic tomography *Photoacoustic Imaging and Spectroscopy* ed L H Wang (Boca Raton, FL: CRC Press) pp 89–101

[2] Andersson L-E 1988 On the determination of a function from spherical averages *SIAM J. Math. Anal.* **19** 214–32

[3] Cohen J and Bleistein H 1979 Velocity inversion procedure for acoustic waves *Geophysics* **44** 1077–85

[4] Courant R and Hilbert D 1962 *Methods of Mathematical Physics* vol 2 (New York: Wiley Interscience)

[5] Denisjuk A 1999 Integral geometry on the family of semi-spheres *Fract. Calc. Appl. Anal.* **2** 31–46

[6] Fawcett J 1985 Inversion of *N*-dimensional spherical averages *SIAM J. Appl. Math.* **45** 336–41

[7] Faridani A, Ritman E L and Smith K T 1992 Local tomography *SIAM J. Appl. Math.* **52** 459–84

[8] Guillemin V 1975 Some remarks on integral geometry *Technical Report* MIT

[9] Guillemin V 1985 On some results of Gelfand in integral geometry *Proc. Symp. Pure Math.* **43** 149–55

[10] Guillemin V and Sternberg S 1977 *Geometric Asymptotics* (Providence, RI: American Mathematical Society)

[11] Haltmeier M, Schuster T and Scherzer O 2005 Filtered backprojection for thermoacoustic computed tomography in spherical geometry *Math. Methods Appl. Sci.* **28** 1919–37

[12] Hörmander L 1971 Fourier integral operators: I *Acta Math.* **127** 79–183

[13] Klein J 2004 Mathematical problems in synthetic aperture radar *PhD Thesis* Westfälische Wilhelms-Universität, Mathematisches Institut, Münster, Germany

[14] Kuchment P and Kunyansky L 2008 Mathematics of thermoacoustic tomography *Eur. J. Appl. Math.* **19** 191–224

[15] Louis A K 1996 Approximate inverse for linear and some nonlinear problems *Inverse Problems* **12** 175–90

[16] Louis A K and Quinto E T 2000 *Local Tomographic Methods in SONAR Surveys on Solution Methods for Inverse Problems (Vienna/New York)* ed D Colton, H Engl, A Louis, J McLaughlin and W Rundell (Berlin: Springer) pp 147–54

[17] Norton S J and Linzer M 1981 Ultrasonic reflectivity imaging in three dimensions: exact inverse scattering solutions for plane, cylindrical, and spherical apertures *IEEE Trans. Biomed. Eng.* **28** 200–2

[18] Palamodov V 2000 Reconstruction from limited data of arc means *J. Fourier Anal. Appl.* **6** 25–42

[19] Petersen B 1983 *Introduction to the Fourier Transform and Pseudo Differential Operators* (Boston, MA: Pittman)

[20] Quinto E T 1980 The dependence of the generalized Radon transform on defining measures *Trans. Am. Math. Soc.* **257** 331–46

[21] Quinto E T 2006 Support theorems for the spherical Radon transform on manifolds *Int. Math. Res. Not.* **2006** 1–17

[22] Rieder A and Schuster T 2003 The approximate inverse in action II: Convergence and stability *Math. Comp.* **72** 1399–415

[23] Rieder A and Schuster T 2004 The approximate inverse in action III: 3D-Doppler tomography *Numer. Math.* **97** 353–78

[24] Schuster T 2007 *The Method of Approximate Inverse: Theory and Applications (Lecture Notes in Mathematics* vol 1906*)* (Berlin: Springer)

[25] Schuster T and Quinto E T 2005 On a regularization scheme for linear operators in distribution spaces with an application to the spherical Radon transform *SIAM J. Appl. Math.* **65** 1369–87

[26] Stein E M 1970 *Singular Integrals and Differentiability Properties of Functions* (Princeton, NJ: Princeton University Press)

[27] Wang L V 2009 *Photoacoustic Imaging and Spectroscopy* (Boca Raton, FL: CRC Press)